Mon. Not. R. Astron. Soc. **318**, 47–57 (2000)

The response of a turbulent accretion disc to an imposed epicyclic shearing motion

Ulf Torkelsson,[1,2★] Gordon I. Ogilvie,[1,3,4] Axel Brandenburg,[3,5,6] James E. Pringle,[1,3] Åke Nordlund[7,8] and Robert F. Stein[9]

[1]*Institute of Astronomy, Madingley Road, Cambridge CB3 0HA*
[2]*Chalmers University of Technology/Göteborg University, Department of Theoretical Physics, Astrophysics Group, S-412 96 Gothenburg, Sweden*
[3]*Isaac Newton Institute for Mathematical Sciences, 20 Clarkson Road, Cambridge CB3 0EH*
[4]*Max-Planck-Institut für Astrophysik, Karl-Schwarzschild-Straße 1, Postfach 1523, D-85740 Garching bei München, Germany*
[5]*Department of Mathematics, University of Newcastle upon Tyne, Newcastle NE1 7RU*
[6]*Nordita, Blegdamsvej 17, DK-2100 Copenhagen Ø, Denmark*
[7]*Theoretical Astrophysics Center, Juliane Maries Vej 30, DK-2100 Copenhagen Ø, Denmark*
[8]*Copenhagen University Observatory, Juliane Maries Vej 30, DK-2100 Copenhagen Ø, Denmark*
[9]*Department of Physics and Astronomy, Michigan State University, East Lansing, MI 48824, USA*

Accepted 2000 April 7. Received 2000 March 29; in original form 1999 July 12

ABSTRACT

We excite an epicyclic motion, the amplitude of which depends on the vertical position, z, in a simulation of a turbulent accretion disc. An epicyclic motion of this kind may be caused by a warping of the disc. By studying how the epicyclic motion decays, we can obtain information about the interaction between the warp and the disc turbulence. A high-amplitude epicyclic motion decays first by exciting inertial waves through a parametric instability, but its subsequent exponential damping may be reproduced by a turbulent viscosity. We estimate the effective viscosity parameter, $\alpha_{\rm v}$, pertaining to such a vertical shear. We also gain new information on the properties of the disc turbulence in general, and measure the usual viscosity parameter, $\alpha_{\rm h}$, pertaining to a horizontal (Keplerian) shear. We find that, as is often assumed in theoretical studies, $\alpha_{\rm v}$ is approximately equal to $\alpha_{\rm h}$ and both are much less than unity, for the field strengths achieved in our local box calculations of turbulence. In view of the smallness ($\sim$0.01) of $\alpha_{\rm v}$ and $\alpha_{\rm h}$ we conclude that for $\beta = p_{\rm gas}/p_{\rm mag} \sim 10$ the time-scale for diffusion or damping of a warp is much shorter than the usual viscous time-scale. Finally, we review the astrophysical implications.

Key words: accretion, accretion discs – instabilities – MHD – turbulence.

1 INTRODUCTION

Warped accretion discs appear in many astrophysical systems. A well-known case is the X-ray binary Her X-1, in which a precessing warped disc is understood to be periodically covering our line of sight to the neutron star, resulting in a 35-d periodicity in the X-ray emission (Tananbaum et al. 1972; Katz 1973; Roberts 1974). A similar phenomenon is believed to occur in a number of other X-ray binaries. In recent years the active galaxy NGC 4258 has received much attention as a warp in the accretion disc has been made visible by a maser source (Miyoshi et al. 1995).

A warp may appear in an accretion disc in response to an external perturber such as a binary companion, but it is also possible that the disc may produce a warp on its own. Pringle (1996) showed that the radiation pressure from the central radiation source may produce a warp in the outer disc. In a related mechanism, the irradiation can drive an outflow from the disc. The force of the wind may then in a similar way excite a warp in the disc (Schandl & Meyer 1994).

Locally, one of the effects of a warp is to induce an epicyclic motion the amplitude of which varies linearly with distance from the mid-plane of the disc. This motion is driven near resonance in a Keplerian disc, and its amplitude and phase are critical in determining the evolution of the warp (Papaloizou & Pringle 1983; Papaloizou & Lin 1995). Depending on the strength of the dissipative process, the warp may either behave as a propagating bending wave or evolve diffusively. In the latter case the amplitude of the epicyclic motion is determined by the dissipative process.

A (possibly) related dissipative process is responsible for driving the inflow and heating the disc by transporting angular momentum outwards. From a theoretical point of view this transport has been described in terms of a viscosity (Shakura & Sunyaev 1973), but the source of the viscosity remained uncertain for a long time. It was clear from the beginning that molecular

★ E-mail: torkel@fy.chalmers.se

viscosity would be insufficient, so one appealed to some form of anomalous viscosity presumably produced by turbulence in the accretion disc. However, the cause of the turbulence could not be found as the Keplerian rotation is hydrodynamically stable according to Rayleigh's criterion.

Eventually Balbus & Hawley (1991) discovered that the Keplerian flow becomes unstable in the presence of a magnetic field. This magnetic shearing instability had already been described by Velikhov (1959) and Chandrasekhar (1960), but it had not been thought applicable in the context of accretion discs before. Several numerical simulations (e.g. Hawley, Gammie & Balbus 1995; Matsumoto & Tajima 1995; Brandenburg et al. 1995; Stone et al. 1996) have demonstrated how this instability generates turbulence in a Keplerian shear flow.

The most important result of these simulations has been to demonstrate that the Maxwell and Reynolds stresses that the turbulence generates will transport angular momentum outwards, thus driving the accretion. The energy source of the turbulence is the Keplerian shear flow, from which the magnetic field taps energy. This energy is then partially dissipated as a result of Ohmic diffusion, but an equal amount of energy is spent on exciting the turbulent motions. The turbulent motions on the other hand give rise to a dynamo, which sustains the magnetic field required by the Balbus–Hawley instability (Brandenburg et al. 1995; Hawley, Gammie & Balbus 1996).

In general the energy of the magnetic field is an order of magnitude larger than the energy of the turbulent velocities, but almost all of the magnetic energy is associated with the toroidal magnetic field, and the poloidal magnetic field components are comparable to the turbulent velocities.

So far none of the simulations has addressed the question of how the turbulence responds to external perturbations or systematic motions that are more complex than a Keplerian shear flow. The purpose of this paper is to begin such an investigation by studying how the turbulence interacts with an imposed shearing epicyclic motion of the type found in a warped disc.

We start this paper by describing the shearing-box approximation of magnetohydrodynamics and summarizing the properties of the epicyclic motion in a shearing box in Section 2. Section 3 is then a description of our simulations of an epicyclic motion. The results of the simulations are then described in Section 4 and briefly summarized in Section 5.

2 MATHEMATICAL FORMULATION

2.1 The local structure of a steady disc

For the intentions of this paper it is sufficient to use a simple model of the vertical structure of a geometrically thin accretion disc. The disc is initially in hydrostatic equilibrium,

$$\frac{\partial p}{\partial z} = \rho g_z, \tag{1}$$

where p is the pressure, ρ the density, and $g_z = -GMz/R_0^3$ the vertical component of the gravity with G the gravitational constant, M the mass of the accreting star, and R_0 the radial distance from the star. For simplicity we assume that the disc material is initially isothermal, and is a perfect gas, so that $p = c_s^2\rho$, where c_s is the isothermal sound speed, which is initially constant. The density distribution is then

$$\rho = \rho_0 \mathrm{e}^{-z^2/H^2}, \tag{2}$$

where the Gaussian scaleheight, H, is given by

$$H^2 = \frac{2c_s^2 R_0^3}{GM}. \tag{3}$$

2.2 Epicyclic motion in the shearing box approximation

In the shearing box approximation a small part of the accretion disc is represented by a Cartesian box which is rotating at the Keplerian angular velocity $\Omega_0 = \sqrt{GM/R_0^3}$. The box uses the coordinates (x,y,z) for the radial, azimuthal and vertical directions, respectively. The Keplerian shear flow within the box is $u_y^{(0)} = -\frac{3}{2}\Omega_0 x$, and we solve for the deviations from the shear flow exclusively. The magnetohydrodynamic (MHD) equations may then be written

$$\frac{\mathcal{D}\rho}{\mathcal{D}t} = -\nabla\cdot(\rho\boldsymbol{u}), \tag{4}$$

$$\frac{\mathcal{D}\boldsymbol{u}}{\mathcal{D}t} = -(\boldsymbol{u}\cdot\nabla)\boldsymbol{u} + \boldsymbol{g} + \boldsymbol{f}(\boldsymbol{u}) - \frac{1}{\rho}\nabla p + \frac{1}{\rho}\boldsymbol{J}\times\boldsymbol{B} + \frac{1}{\rho}\nabla\cdot(2\nu\rho\boldsymbol{S}), \tag{5}$$

$$\frac{\mathcal{D}\boldsymbol{B}}{\mathcal{D}t} = \nabla\times(\boldsymbol{u}\times\boldsymbol{B}) - \nabla\times\eta\mu_0\boldsymbol{J}, \tag{6}$$

$$\frac{\mathcal{D}e}{\mathcal{D}t} = -(\boldsymbol{u}\cdot\nabla)e - \frac{p}{\rho}\nabla\cdot\boldsymbol{u} + \frac{1}{\rho}\nabla\cdot(\chi\rho\nabla e) + 2\nu\boldsymbol{S}^2 + \frac{\eta\mu_0}{\rho}\boldsymbol{J}^2 + Q, \tag{7}$$

where $\mathcal{D}/\mathcal{D}t = \partial/\partial t + u_y^{(0)}\partial/\partial y$ includes the advection by the shear flow, ρ is the density, $\boldsymbol{u}$ the deviation from the Keplerian shear flow, p the pressure, $\boldsymbol{f}(\boldsymbol{u}) = \Omega_0(2u_y, -\frac{1}{2}u_x, 0)$ the inertial force, $\boldsymbol{B}$ the magnetic field, $\boldsymbol{J} = \nabla\times\boldsymbol{B}/\mu_0$ the current, μ_0 the permeability of free space, ν the viscosity, $S_{ij} = \frac{1}{2}\left(u_{i,j} + u_{j,i} - \frac{2}{3}\delta_{ij}u_{k,k}\right)$ the trace-free rate of strain tensor, η the magnetic diffusivity, e the internal energy, χ the thermal conductivity, and Q is a cooling function. The radial component of the gravity cancels against the centrifugal force, and the remaining vertical component is $\boldsymbol{g} = -\Omega_0^2 z\hat{\boldsymbol{z}}$. We adopt the equation of state for an ideal gas, $p = (\gamma - 1)\rho e$.

When the horizontal components of the momentum equation (5) are averaged over horizontal layers (an operation denoted by angle brackets), we obtain

$$\frac{\partial}{\partial t}\langle\rho u_x\rangle = 2\Omega_0\langle\rho u_y\rangle - \frac{\partial}{\partial z}\langle\rho u_x u_z\rangle + \frac{\partial}{\partial z}\left\langle\frac{B_x B_z}{\mu_0}\right\rangle, \tag{8}$$

$$\frac{\partial}{\partial t}\langle\rho u_y\rangle = -\frac{1}{2}\Omega_0\langle\rho u_x\rangle - \frac{\partial}{\partial z}\langle\rho u_y u_z\rangle + \frac{\partial}{\partial z}\left\langle\frac{B_y B_z}{\mu_0}\right\rangle. \tag{9}$$

The explicit viscosity, which is very small, has been neglected here. These equations contain vertical derivatives of components of the turbulent Reynolds and Maxwell stress tensors, distinct from the xy components that drive the accretion.

We initially neglect the turbulent stresses and obtain the solution

$$\langle\rho u_x\rangle = \rho_0(z)\tilde{u}_0(z)\cos(\Omega_0 t), \tag{10}$$

$$\langle\rho u_y\rangle = -\tfrac{1}{2}\rho_0(z)\tilde{u}_0(z)\sin(\Omega_0 t), \tag{11}$$

which describes an epicyclic motion. Here $\rho_0(z)$ is the initial density profile. The initial velocity amplitude $\tilde{u}_0$ is an arbitrary function of z. For the simulations in this paper we will take $\tilde{u}_0(z) \propto \sin(kz)$, where $k = \pi/L_z$, and $-\frac{1}{2}L_z \le z \le \frac{1}{2}L_z$ is the vertical extent of our shearing box. This velocity profile is

compatible with the stress-free boundary conditions that we employ in our numerical simulations, and gives a fair representation of a linear profile close to the mid-plane of the disc.

The kinetic energy of the epicyclic motion is not conserved, but the square of the epicyclic momentum

$$E(z,t) = \tfrac{1}{2}\langle \rho u_x\rangle^2 + 2\langle \rho u_y\rangle^2, \tag{12}$$

is conserved in the absence of turbulent stresses. By multiplying equation (8) by $\langle \rho u_x\rangle$, and equation (9) by $4\langle \rho u_y\rangle$ we obtain

$$\frac{\partial E}{\partial t} = F_u + F_B, \tag{13}$$

where

$$F_u = -\langle \rho u_x\rangle \frac{\partial}{\partial z}\langle \rho u_x u_z\rangle - 4\langle \rho u_y\rangle \frac{\partial}{\partial z}\langle \rho u_y u_z\rangle \tag{14}$$

and

$$F_B = \langle \rho u_x\rangle \frac{\partial}{\partial z}\left\langle \frac{B_x B_z}{\mu_0}\right\rangle + 4\langle \rho u_y\rangle \frac{\partial}{\partial z}\left\langle \frac{B_y B_z}{\mu_0}\right\rangle \tag{15}$$

represent the 'rates of working' of the Reynolds and Maxwell stresses, respectively, on the epicyclic oscillator. We may expect that both F_u and F_B are negative, but by measuring them in the simulation we may determine the relative importance of the Reynolds and Maxwell stresses in damping the epicyclic motion. We will also refer to an epicyclic velocity amplitude

$$\tilde{u} = \sqrt{\langle u_x\rangle^2 + 4\langle u_y\rangle^2}. \tag{16}$$

2.3 Theoretical expectations

The detailed fluid dynamics of a warped accretion disc has been discussed by, e.g., Papaloizou & Pringle (1983), Papaloizou & Lin (1995) and Ogilvie (1999). The dominant motion is circular Keplerian motion, but the orbital plane varies continuously with radius r and time t. This may conveniently be described by the tilt vector $\ell(r,t)$, which is a unit vector parallel to the local angular momentum of the disc annulus at radius r. A dimensionless measure of the amplitude of the warp is then $A = |\partial \ell/\partial \ln r|$.

In the absence of a detailed understanding of the turbulent stresses in an accretion disc, it is invariably assumed that the turbulence acts as an isotropic effective viscosity in the sense of the Navier–Stokes equation. In such an approach the dynamic viscosity is often parametrized as

$$\mu = \alpha p/\Omega_0, \tag{17}$$

where α is a dimensionless parameter (Shakura & Sunyaev 1973). Although it is now possible to simulate the local turbulence in an accretion disc, this form of phenomenological description of the turbulent stress is still valuable as it is not yet possible to study simultaneously both the small-scale turbulence and the global dynamics of the accretion disc in a numerical simulation. One of the goals of this paper is to test the validity of this hypothesis by comparing the predictions of the viscous model, as summarized below, with the results of the numerical model. We generalize the viscosity prescription by allowing, in a simple way, for the possibility that the effective viscosity is anisotropic (cf. Terquem 1998). The parameter $\alpha_{\rm h}$ pertaining to 'horizontal' shear (i.e. horizontal–horizontal components of the rate-of-strain tensor, such as the Keplerian shear) may be different from the parameter $\alpha_{\rm v}$ pertaining to 'vertical' shear (i.e. horizontal–vertical components of the rate-of-strain tensor, such as the shearing epicyclic motion).

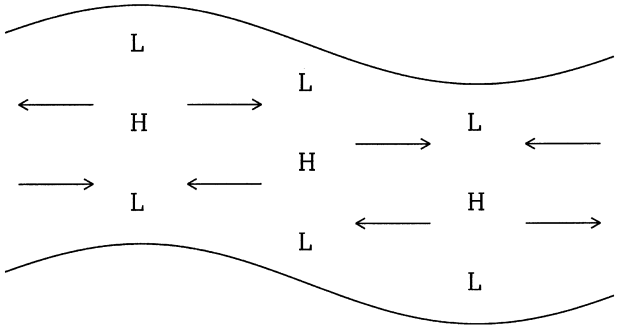

Figure 1. Owing to the stratification there appear horizontal pressure gradients in the warped disc. These gradients excite the epicyclic motion (arrows indicate forces, not velocities).

Owing to the pressure stratification, resulting from the vertical hydrostatic equilibrium, in a warped disc there are strong *horizontal* pressure gradients (Fig. 1) that generate horizontal accelerations of order $A\Omega_0^2 z$, which oscillate at the local orbital frequency, as viewed in a frame corotating with the fluid. In a Keplerian disc the frequency of the horizontal pressure gradients coincides with the natural frequency of the resulting epicyclic motion, and a resonance occurs. The amplitude of the resulting epicyclic motion depends on the amount of dissipation present. At low viscosities, $\alpha_{\rm v} \lesssim H/r$, the amplitude is limited by the coupling of the epicyclic motion to the vertical motion in a propagating bending wave, which transports energy away. At higher viscosities the amplitude is limited by a balance between the forcing and the viscous dissipation, and the warp evolves diffusively (Papaloizou & Pringle 1983). When $H/r \lesssim \alpha_{\rm v} \ll 1$ the amplitude of the epicyclic motion is

$$u_x \propto u_y \propto \frac{A\Omega_0 z}{\alpha_{\rm v}}. \tag{18}$$

The resulting hydrodynamic stresses $\overline{\rho u_x u_z}$ and $\overline{\rho u_y u_z}$ (overbars denote averages over the orbital time-scale), which tend to flatten out the disc, are also proportional to $\alpha_{\rm v}^{-1}A$ and therefore dominate over the stresses $\propto \alpha_{\rm v} A$ caused by small-scale turbulent motions, which would have the same effect. It is for this reason that the time-scale for flattening a warped disc is anomalously short compared to the usual viscous time-scale, by a factor of approximately $2\alpha_{\rm h}\alpha_{\rm v}$. (For more details, see Papaloizou & Pringle 1983 and Ogilvie 1999. In these papers it was assumed that $\alpha_{\rm h} = \alpha_{\rm v}$.)

We aim to measure both $\alpha_{\rm h}$ and $\alpha_{\rm v}$ in the simulations. The first may be obtained through the relation

$$\left\langle \rho u_x u_y - \frac{B_x B_y}{\mu_0}\right\rangle_{\rm V} = \frac{3}{2}\alpha_{\rm h}\langle p\rangle_{\rm V}, \tag{19}$$

which follows by identifying the total turbulent xy stress with the effective viscous xy stress resulting from the viscosity (17) acting on the Keplerian shear (note that the definition of $\alpha_{\rm h}$ differs from that of $\alpha_{\rm SS}$ in Brandenburg et al. 1995 by a factor $\sqrt{2}$). Here the average is over the entire computational volume.

The coefficient $\alpha_{\rm v}$ may be obtained by measuring the damping time of the epicyclic motion. In the shearing-box approximation, the horizontal components of the Navier–Stokes equation for a free epicyclic motion decaying under the action of

viscosity are

$$\frac{\partial u_x}{\partial t} = 2\Omega_0 u_y + \frac{1}{\rho}\frac{\partial}{\partial z}\left(\frac{\alpha_{\rm v} p}{\Omega_0}\frac{\partial u_x}{\partial z}\right), \tag{20}$$

$$\frac{\partial u_y}{\partial t} = -\frac{1}{2}\Omega_0 u_x + \frac{1}{\rho}\frac{\partial}{\partial z}\left(\frac{\alpha_{\rm v} p}{\Omega_0}\frac{\partial u_y}{\partial z}\right). \tag{21}$$

Under the assumptions that $\alpha_{\rm v}$ and $\partial_z \boldsymbol{u}$ are independent of z and that the disc is vertically in hydrostatic equilibrium, these equations have the exact solution

$$u_x = C\Omega_0 z {\rm e}^{-t/\tau}\cos(\Omega_0 t), \tag{22}$$

$$u_y = -\tfrac{1}{2} C\Omega_0 z {\rm e}^{-t/\tau}\sin(\Omega_0 t). \tag{23}$$

where C is a dimensionless constant and

$$\tau = \frac{1}{\alpha_{\rm v}\Omega_0} \tag{24}$$

is the damping time. Admittedly it is already believed that $\alpha_{\rm h}$ is not independent of z (Brandenburg et al. 1996) and therefore $\alpha_{\rm v}$ may not be either. Also, our velocity profile is not exactly proportional to z. However, it is in fact the damping time that matters for the application to a warped disc, and the solution that we describe above is in a sense the fundamental mode of the epicyclic shear flow in a warped disc.

It might be argued that the decaying epicyclic motion is fundamentally impossible in the presence of MHD turbulence. After all, the magnetorotational instability works because a magnetic coupling between two fluid elements executing an epicyclic motion allows an exchange of angular momentum that destabilizes the motion. However, we argue that the epicyclic motion must be *re-stabilized* in the non-linear turbulent state. Otherwise epicyclic motions, which are continuously and randomly forced by the turbulence, would grow indefinitely (Balbus & Hawley 1998). In fact they last only a few orbits, as discussed in Section 3.2 (below). Moreover, our numerical results demonstrate without any doubt that the shearing epicyclic motion is possible, and does decay in the presence of MHD turbulence.

A further theoretical expectation is as follows. In an inviscid disc, the epicyclic motion can decay by exciting inertial waves through a parametric instability (Gammie, Goodman & Ogilvie 2000). In the optimal case, the signature of these waves is motion at 30° to the vertical, while the wave vector is inclined at 60° to the vertical. The characteristic local growth rate of the instability is

$$\gamma = \frac{3\sqrt{3}}{16}\left|\frac{\partial u_x}{\partial z}\right|. \tag{25}$$

This instability can lead to a rapid damping of a warp, but may be somewhat delicate as it relies on properties of the inertial-wave spectrum. It is important to determine whether it occurs in the presence of MHD turbulence.

3 NUMERICAL SIMULATIONS

3.1 Computational method

We use the code by Nordlund & Stein (1990) with the modifications that were described by Brandenburg et al. (1995). The code solves the MHD equations for $\ln\rho$, $\boldsymbol{u}$, e and the vector potential $\boldsymbol{A}$, which gives the magnetic field via $\boldsymbol{B} = \nabla\times\boldsymbol{A}$. For the (radial) azimuthal boundaries we use (sliding) periodic boundary conditions. The vertical boundaries are assumed to be impenetrable and stress-free. Unlike our earlier studies, we now adopt perfectly conducting vertical boundary conditions for the magnetic field. Thus we have

$$\frac{\partial u_x}{\partial z} = \frac{\partial u_y}{\partial z} = u_z = 0, \tag{26}$$

and

$$\frac{\partial B_x}{\partial z} = \frac{\partial B_y}{\partial z} = B_z = 0. \tag{27}$$

We choose units such that $H = GM = 1$. Density is normalized so that initially $\rho = 1$ at the mid-plane, and we measure the magnetic field strength in velocity units, which allows us to set $\mu_0 = 1$. The disc may be considered to be thin by the assumptions of our model, and the results will thus not depend on the value of R_0. We choose to set $R_0 = 10$ in our units, which gives the orbital period $T_0 = 2\pi/\Omega_0 = 199$, and the mean internal energy $e = 7.4\times10^{-4}$. The size of the box is $L_x : L_y : L_z = 1 : 2\pi : 4$, where x and z vary between $\pm\frac{1}{2}L_x$ and $\pm\frac{1}{2}L_z$, respectively, and y goes from 0 to L_y. The number of grid points is $N_x\times N_y\times N_z$. To stop the box from heating up during the simulation we introduce the cooling function

$$Q = -\sigma_{\rm cool}(e - e_0), \tag{28}$$

where $\sigma_{\rm cool}$ is the cooling rate, which typically corresponds to a time-scale of 1.5 orbital periods, and e_0 is the internal energy of an isothermal disc.

Although the Balbus–Hawley instability appears readily in a numerical simulation, experience has taught us that the initial conditions must be chosen carefully in order for the instability to develop into sustained turbulence, unless the initial magnetic field has a net flux. In particular, the initial field strength should be chosen such that the Alfvén speed is close to the sound speed. Otherwise the field becomes too weak before the dynamo effect sets in. Experience has shown that after about 50 orbital periods the simulations are independent of the details of the initial conditions, which is typical of turbulence in general. To save time we started the simulations in this paper from a snapshot of a previous simulation (Brandenburg 1999). The origin of this snapshot goes back to the simulations by Brandenburg et al. (1995). In those simulations we started from a magnetic field of the form $\hat{z}B_0\sin(2\pi x/L_x)$ (at that time we employed boundary conditions that constrained the magnetic field to be vertical on the upper and lower boundaries). B_0 was chosen such that $\beta = 2\mu_0 p/B_0^2 = 100$ on average in the shearing box. A snapshot from an evolved stage of one of these simulations was later relaxed for about 55 orbital periods to fit the perfectly conducting upper and lower boundaries of Brandenburg (1999). For the purposes of this paper a snapshot from the new simulation was modified in the following way. For every horizontal layer in the snapshot we subtract the mean horizontal velocity and then add a net radial flow of the form

$$u_x = u_0\sin\left(\frac{\pi z}{L_z}\right). \tag{29}$$

Two things that should be kept in mind here are that the previous simulations have been run long enough that the current snapshot has lost its memory of its original initial conditions, and that in spite of all the modifications there is still no net magnetic flux in the shearing box. The number of grid points and u_0 for the different runs are given in Table 1. u_0 should be compared to the

Table 1. Specification of numerical simulations: the number of grid points are given by $N_x \times N_y \times N_z$, and the amplitude of the initial velocity perturbation is u_0. Note that all Runs except Run 4 starts from a snapshot of a previous simulation of turbulence in an accretion disc. Run 4 starts from a state with no turbulent motions.

Run	$N_x \times N_y \times N_z$	u_0
0	$31 \times 63 \times 63$	0.0
1	$31 \times 63 \times 63$	0.011
1b	$63 \times 127 \times 127$	0.011
2	$31 \times 63 \times 63$	0.095
3	$63 \times 127 \times 127$	0.095
4	$63 \times 127 \times 127$	0.095

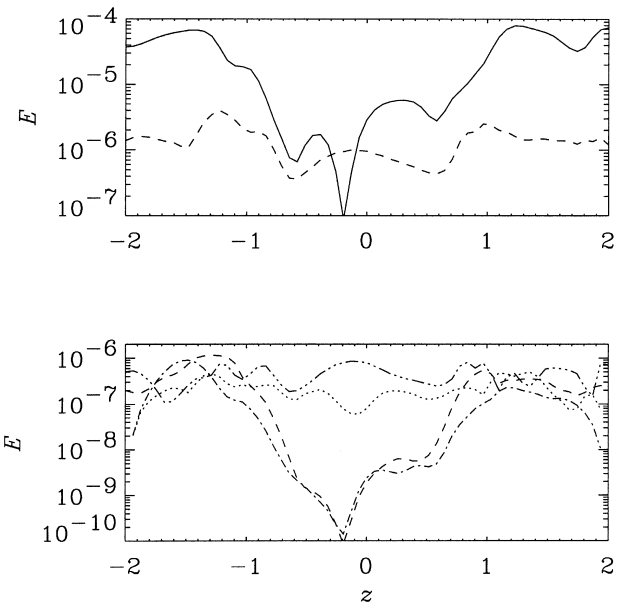

Figure 2. Top: The magnetic (solid line) and kinetic (dashed line) turbulent energies as a function of z at the beginning of Run 0. The energies are completely dominated by the contributions from the y-components of the magnetic field, and velocity, respectively. Bottom: $B_x^2/2$ (dashed line), $B_z^2/2$ (dot-dashed line), $\rho u_x^2/2$ (triple-dotted dashed line) and $\rho u_z^2/2$ (dotted line) as a function of z.

adiabatic sound speed which is 0.029. We include one run, Run 0, in which we do not excite an epicyclic motion, as a reference.

3.2 Results

We start by looking at Run 0. In this case we have not modified the velocity field, so that Run 0 represents the typical properties of the turbulence. The turbulence is fully developed at the beginning of our study, meaning that the shearing box does not remember its initial state any longer. We plot the vertical distributions of the magnetic and turbulent kinetic energies in Fig. 2. The kinetic energy is independent of the vertical coordinate z while the magnetic energy has a minimum close to the mid-plane. It is a typical property of all our simulations that the magnetic energy is up to an order of magnitude larger than the turbulent kinetic

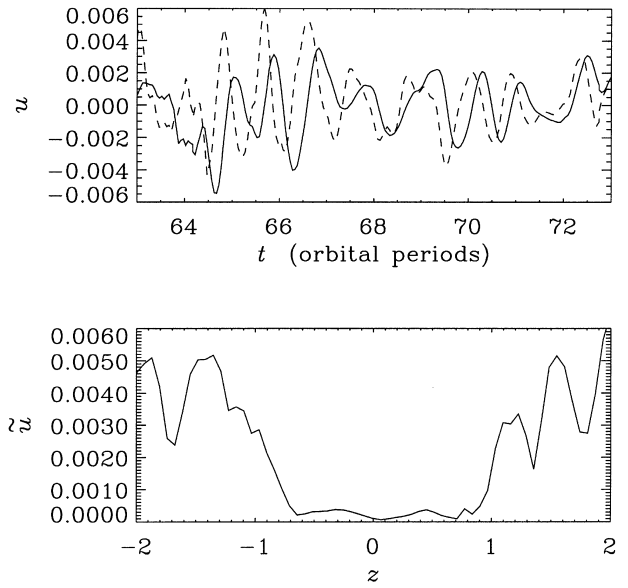

Figure 3. Top: $\langle u_x \rangle$ (solid line) and $2\langle u_y \rangle$ (dashed line) as a function of time at $z = 1.55$ for Run 0. The plot shows that epicyclic motions of amplitude $\sim$0.005 lasting for a couple of orbits appear spontaneously in the disc. Bottom: $\tilde{u}$ as a function of z at $t = 66.7$ orbital periods.

energy, but the magnetic energy is still an order of magnitude smaller than the internal energy, the mean density of which as stated above is 7.4×10^{-4}. A property of both the magnetic and turbulent kinetic energies is that they are completely dominated by the contributions from the azimuthal components of the magnetic field and turbulent velocity, respectively. The other components of the turbulent velocity and magnetic field make about equal contributions to the energy density far from the mid-plane of the disc.

The turbulence generates epicyclic motions with amplitudes $\sim$0.004 lasting for a couple of orbital periods (Fig. 3). The epicyclic velocity amplitude $\tilde{u}$ (see equation 16) is peaked towards the surfaces of the accretion disc (cf. Fig. 3, bottom). Overall these motions complicate the analysis of the rest of our numerical simulations, and force us to excite motions with amplitudes significantly larger than those of the motions produced by the turbulence.

Fig. 4 shows the mean horizontal motion of Run 1b. At the start of the simulation we added a radial velocity of amplitude 0.011. Far from the mid-plane, the imposed epicyclic motion is comparable to that generated by the turbulence, and it becomes virtually impossible to identify a phase of exponential decay. Closer to the mid-plane, the imposed epicyclic motion is initially unaffected by the turbulence. After seven or eight orbital periods a damping sets in, but the net damping before the turbulence starts to reinforce the epicyclic motion is less than a factor of two. By looking at the volume average of the square of the epicyclic momentum, $\langle E \rangle_V$, (Fig. 5) we find a clear trend. The epicyclic motion is obviously damped, and by fitting an exponential we obtain an e-folding time-scale of 17.8 orbital periods for $\langle E \rangle_V$, corresponding to a time-scale of 35.6 orbital periods for the momentum, but the damping is not described accurately by an exponential. Initially the damping is much slower than the fitted exponential, while at the end it is faster.

The analysis becomes more straightforward in Run 3, where we excite a motion of amplitude 0.095. There is then a sufficient

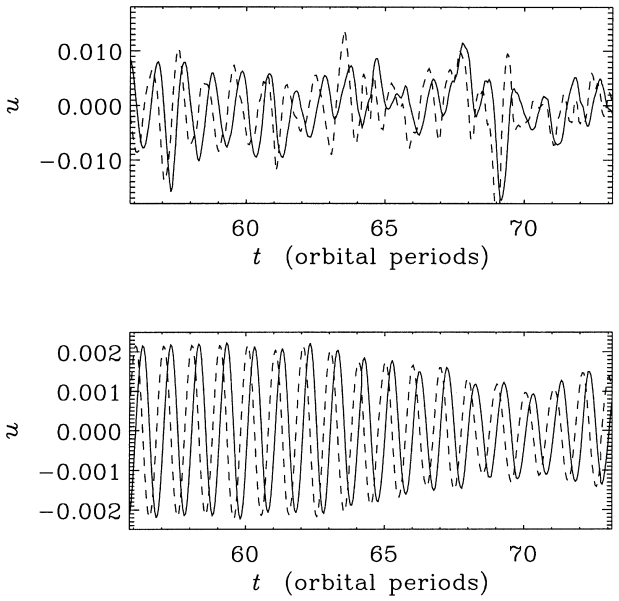

Figure 4. $\langle u_x \rangle$ (solid line) and $2\langle u_y \rangle$ (dashed line) as a function of time at $z = 1.17$ (top) and $z = -0.25$ (bottom) of Run 1b. The damping time-scale in the lower plot during the interval 63 to 68 orbital periods is 15.5 orbital periods.

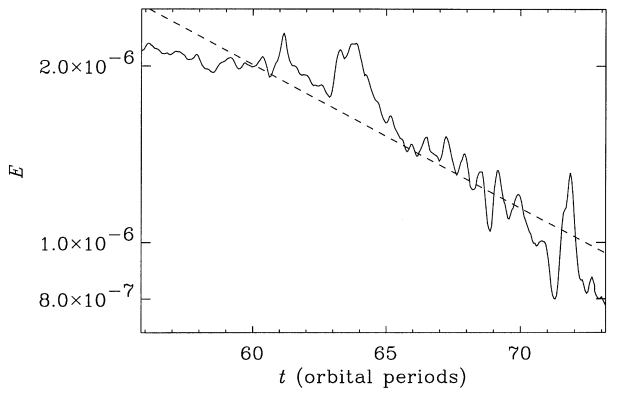

Figure 5. $\langle E \rangle_V$, the square of the epicyclic momentum, as a function of time for Run 1b. The dashed line is a fit with an exponential to $\langle E \rangle_V$. The e-folding time-scale of the exponential is 17.8 orbital periods.

dynamic range between the epicyclic and turbulent motions. We show the vertical variation of $\tilde{u}$ at four different times in Fig. 6, and plot it as a function of time at three different heights; $z = 1.52$, $z = 0.89$ and $z = 0.44$, in Fig. 7. Fig. 6 shows that the damping sets in first at the surfaces, while for $|z| < 1$ there is essentially no damping during the first two orbital periods (Fig. 7). There is then a brief period of rapid damping between $t = 58\,T_0$ and $t = 60\,T_0$ throughout the box, especially for small $|z|$ where $\tilde{u}$ may drop by a factor of 2. This is followed by a period of exponential decay, but after $t = 75\,T_0$ it becomes difficult to follow the epicyclic motion, as the influence of the random turbulence on $\tilde{u}$ becomes significant, in particular close to the mid-plane, where $\tilde{u}$ is small in any case. We estimate the damping time, $\tau = (\mathrm{d} \ln \tilde{u}/\mathrm{d}t)^{-1}$ by fitting exponentials to $\tilde{u}$ in the interval $60\,T_0 < t < 75\,T_0$. Averaged over the box we get $\tau = 25 \pm 8\,T_0$, which corresponds to $\alpha_v = 0.006 \pm 0.002$ according to equation (24).

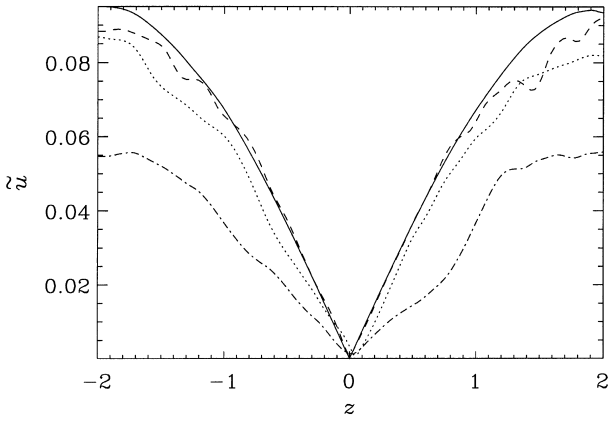

Figure 6. $\tilde{u}$ as a function of z at $t = 55.8\,T_0$ (solid line), $57.1\,T_0$ (dashed line), $58.4\,T_0$ (dotted line), and $60.9\,T_0$ (dot-dashed line) for Run 3.

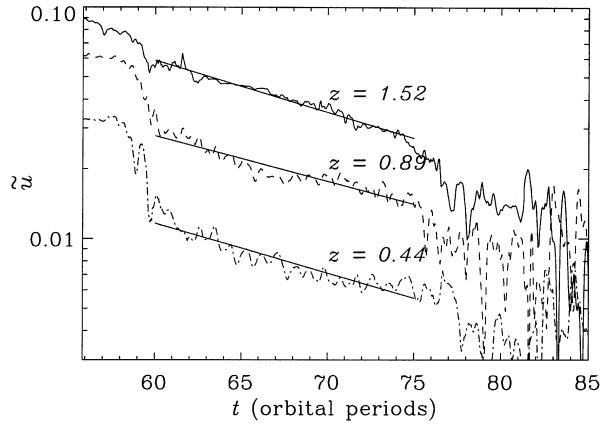

Figure 7. The amplitude of the epicyclic motion in Run 3, $\tilde{u}$, as a function of t on three horizontal planes: $z = 1.52$ (solid line), $z = 0.89$ (dashed line) and $z = 0.44$ (dot-dashed line). The straight lines are exponential functions that have been fitted for the interval $60\,T_0 < t < 75\,T_0$. The e-folding time-scales of the exponentials starting from the top are $19.4\,T_0$, $22.1\,T_0$ and $20.2\,T_0$, respectively. The epicyclic motion was added to the box at $t = 55.7\,T_0$.

We may determine the influence of the Maxwell and Reynolds stresses on the shear flow by plotting F_u and F_B as functions of time (Fig. 8). The sharp peak in F_u coincides with the parametric decay of the epicyclic motion to inertial waves (see Section 4.1, below). As this is a hydrodynamic process it is not surprising that $F_u > F_B$, but it was not expected that F_u would remain the dominating effect at later times, since at the same time it is the Maxwell stress that is driving the radial accretion flow.

The accretion itself is driven by the $\langle \rho u_x u_y - B_x B_y \rangle$ stresses. We plot the moving time averages of the vertical average of the accretion-driving stress of Run 3 in Fig. 9, and as a comparison that of Run 0 in Fig. 10. In the beginning of Run 3 the Reynolds stress is modulated on a time-scale of half the orbital period. This modulation is an artefact of the damping of the epicyclic motion and dies out with time. The Maxwell stress becomes significantly stronger than the Reynolds stress once the epicyclic motion has vanished. Later the stresses vary in phase with each other, as they do all the time in Run 0. The main difference between Run 0 and the end of Run 3 is that the stresses are 2–3 times larger in Run 3. We calculate α_h for Run 3 by dividing the stresses by $\frac{3}{2}\overline{\langle p \rangle_V}$ (Fig. 11). One should take note that the simulations in this paper

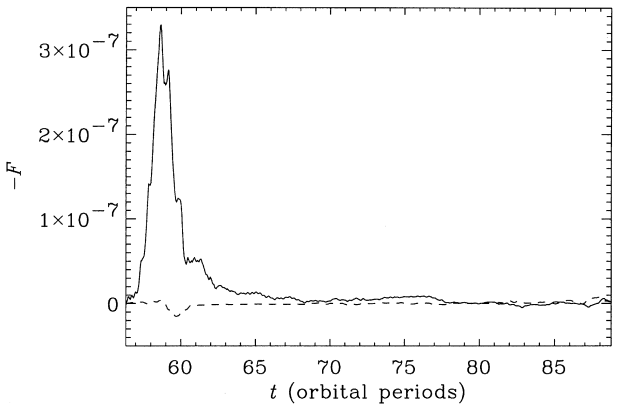

Figure 8. $-\overline{\langle F_u \rangle_{\rm V}}$ (solid line) and $-\overline{\langle F_B \rangle_{\rm V}}$ (dashed line) as a function of time for Run 3.

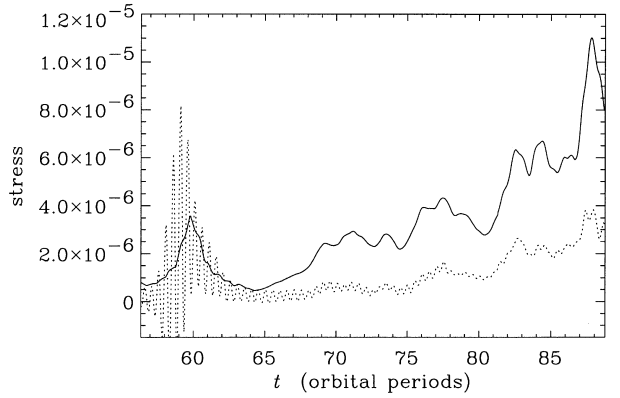

Figure 9. $-\overline{\langle B_x B_y \rangle_{\rm V}}$ (solid line) and $\overline{\langle \rho u_x u_y \rangle_{\rm V}}$ of Run 3.

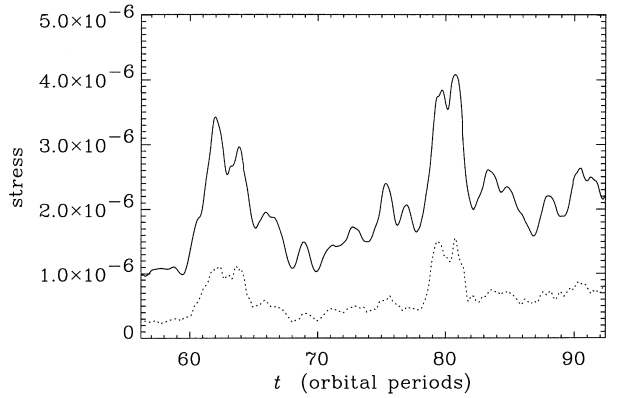

Figure 10. $-\overline{\langle B_x B_y \rangle_{\rm V}}$ (solid line) and $\overline{\langle \rho u_x u_y \rangle_{\rm V}}$ of Run 0.

are too short to derive $\alpha_{\rm h}$ with high statistical significance (cf. Brandenburg et al. 1995), but our results do show that $\alpha_{\rm h}$ varies in phase with the stress. In other words, the pressure variations are smaller (the pressure increases by 50 per cent during the course of the simulation) than the stress variations, which is not what we expect from equation (19). The lack of a correlation between the stress and the pressure is even more evident in Run 0, in which the pressure never varies by more than 5 per cent.

In our previous work (Brandenburg et al. 1995) we found that the toroidal magnetic flux reversed its direction about every 30

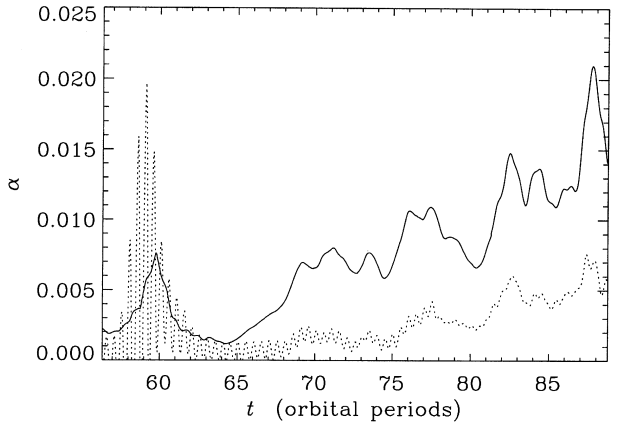

Figure 11. $\alpha_{\rm h}$ is calculated by dividing $-\overline{\langle B_x B_y \rangle_{\rm V}}$ (solid line) and $\overline{\langle \rho u_x u_y \rangle_{\rm V}}$ (dashed line) of Run 3 with $\frac{3}{2}\overline{\langle p \rangle_{\rm V}}$.

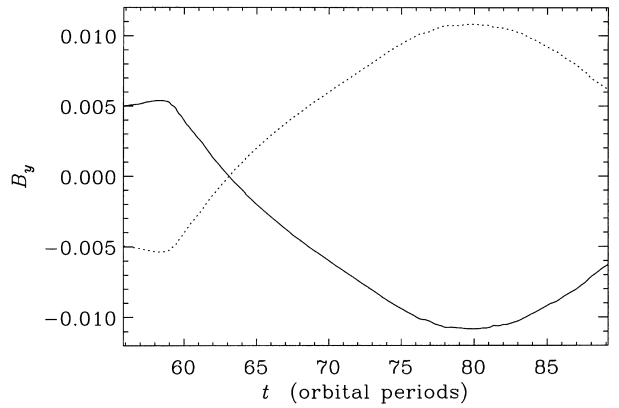

Figure 12. B_y averaged over the upper half (solid line) and lower half (dotted line) of the box of Run 3.

orbital periods. With the perfect conductor boundary conditions that we have assumed in this paper, such field reversals are not allowed, since the boundary conditions conserve the toroidal magnetic flux (e.g. Brandenburg 1999). In all of our simulations we made sure that the toroidal magnetic flux was 0. However, the azimuthal magnetic field organized itself in such a way that it is largely antisymmetric with respect to the mid-plane. That is, considering separately the upper and lower halves of the box, we may still find significant toroidal fluxes, but with opposite directions. These fluxes may still be reversed by the turbulent dynamo as we found in Run 3 (Fig. 12).

3.3 Dependence on u_0 and on the resolution

There is some evidence from comparing Runs 1b and 3 that the damping time-scale decreases as u_0 is increased, but it is more difficult to study the damping of the epicyclic motion for a smaller u_0, as the turbulence may excite epicyclic motions on its own. The randomly excited motions swamp the epicyclic motion that we are studying. The quantitative results from Runs 1 and 1b are therefore more uncertain. In other respects the turbulent stresses of Runs 1 and 1b are more similar to those of Run 0 than to those of Run 3.

On the other hand there are significant differences between Runs 2 and 3, which differ only in terms of the grid resolution.

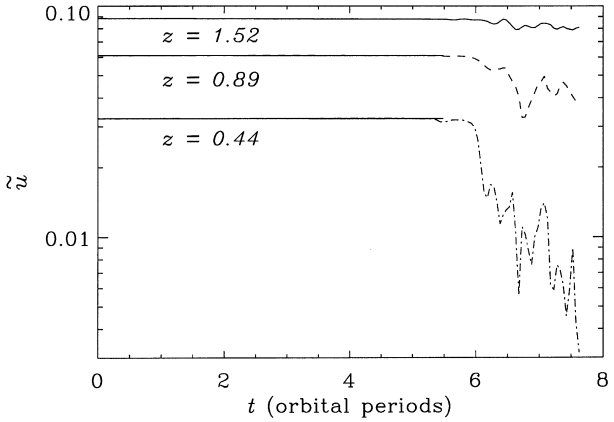

Figure 13. The amplitude of the epicyclic motion of Run 4, $\tilde{u}$, as a function of t on three horizontal planes: $z = 1.52$ (solid line), $z = 0.89$ (dashed line), and $z = 0.44$ (dot-dashed line). The straight lines are exponential functions that have been fitted for the interval $0 < t < 5.5T_0$. The e-folding time-scales of the exponentials starting from the top are $640T_0$, $4\,700T_0$ and $2\,800T_0$, respectively.

The magnetic field decays rapidly in Run 2, and only the toroidal field recovers towards the end of the simulation. In the absence of a poloidal magnetic field there is no magnetic stress, and therefore the disc cannot extract energy from the shear flow. Consequently there is no turbulent heating in Run 2, and the disc settles down to an isothermal state. Apparently the turbulence is killed by the numerical diffusion in Run 2. This demonstrates that the minimal resolution which is required in the simulation depends on the amplitude $\tilde{u}_0$. A simulation with an imposed velocity $\tilde{u}_0$ with an amplitude significantly larger than that of the turbulence requires a finer resolution than a simulation of undisturbed turbulence. Run 2 failed because the imposed velocity field in combination with the limited resolution generated a numerical diffusion large enough to kill the turbulence. This was not a problem in Run 1, where the amplitude $\tilde{u}_0$ is much smaller.

To check the influence of numerical diffusion on Run 3 we imposed the same velocity profile as in Run 3 on a shearing box without any turbulence (Run 4). We plot the evolution of $\tilde{u}$ in Fig. 13. We fitted exponential functions to $\tilde{u}$ for the interval 0–5.5 orbital periods. The shortest e-folding time we obtained over this interval was 640 orbital periods for $z = 1.52$. Closer to the mid-plane, the e-folding time-scale was several thousand orbital periods. These numbers are indicative of the effect of numerical diffusion in the simulations. The strong damping at $t = 6$ orbital periods is *not* the result of numerical diffusion, rather it is caused by a *physical* parametric instability (see Section 4.1, below) that, in this case, has been triggered by numerical noise.

4 DISCUSSION

For the purposes of the following discussion we now summarize our main results.

(1) In Runs 3 and 4 the initial damping of the epicyclic motion is caused by its parametric decay to inertial waves (see Section 4.1, below).

(2) Apart from this, the epicyclic motion experiences approximately exponential damping through interaction with the turbulence. The e-folding time-scale is about 25 orbital periods, which may be interpreted as $\alpha_{\rm v} = 0.006$.

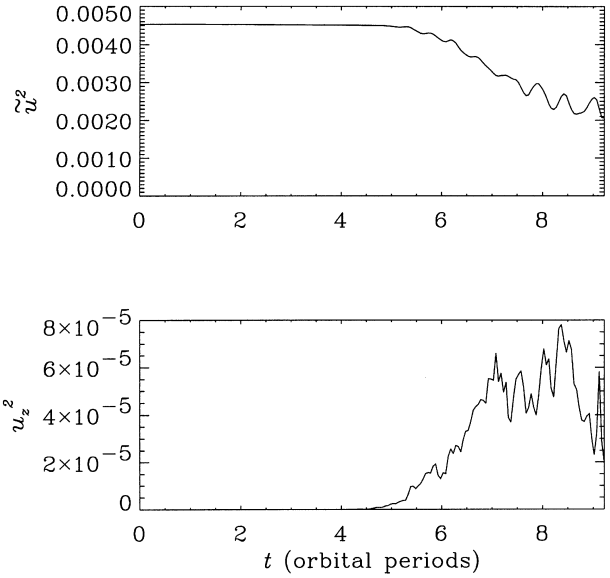

Figure 14. $\langle \tilde{u}^2 \rangle_{\rm V}$ (top) and $\langle u_z^2 \rangle_{\rm V}$ (bottom) for a two-dimensional simulation of parametric decay. The decay of the epicyclic motion excites a vertical motion.

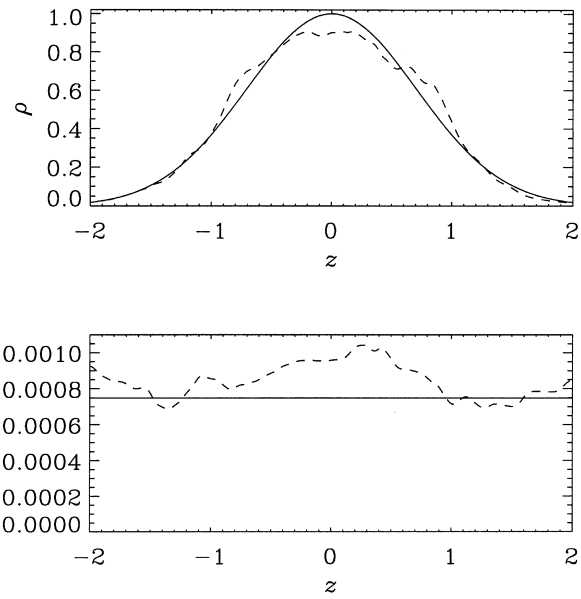

Figure 15. The density $\langle \rho \rangle$ (top) and internal energy $\langle e \rangle$ (bottom) as functions of z at the start of the two-dimensional simulation (solid line) and after 8.97 orbital periods (dashed line).

(3) $\alpha_{\rm h}$, which describes the accretion-driving stress $\langle \rho u_x u_y - B_x B_y \rangle$ is of comparable size.

4.1 Parametric decay to inertial waves

Gammie et al. (2000) predicted the occurrence of a parametric instability in epicyclic shear flows. The shear flow should excite pairs of inertial waves that propagate at roughly a 30° angle to the vertical, and involve vertical as well as horizontal motions. To elucidate the dynamics of the parametric instability we make use of a two-dimensional hydrodynamic simulation of an epicyclic shear flow. Our two-dimensional xz plane has the same extension

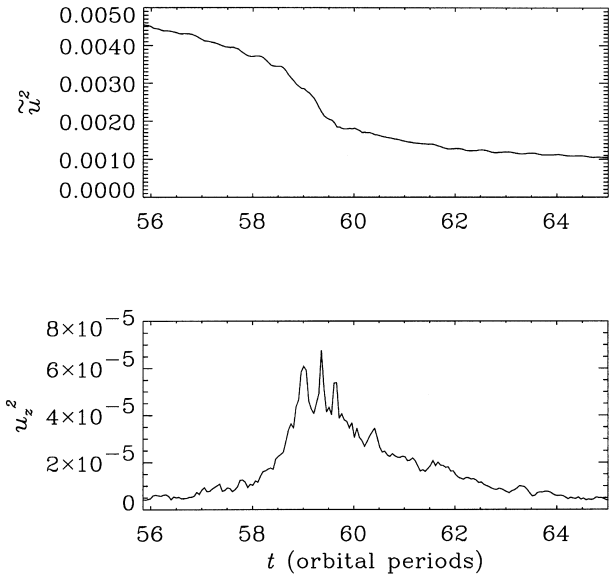

Figure 16. $\langle \tilde{u}^2 \rangle_V$ (top) and $\langle u_z^2 \rangle_V$ (bottom) for Run 3.

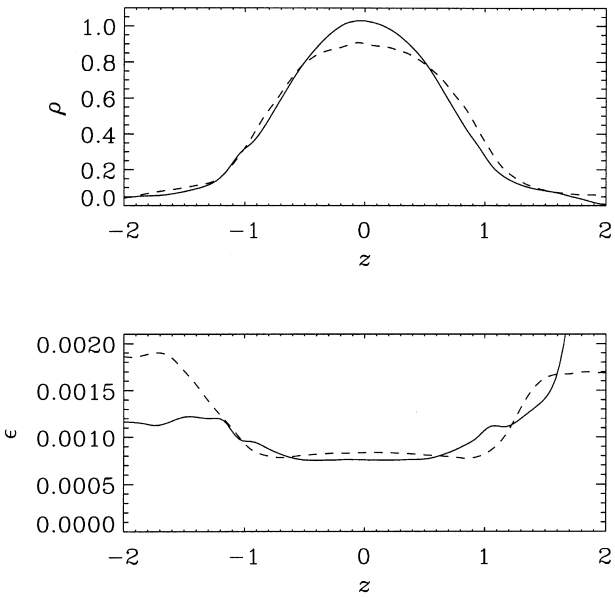

Figure 17. The density $\langle \rho \rangle$ (top) and internal energy $\langle e \rangle$ (bottom) as functions of z for Run 3 at $t = 55.8$ (solid line) and $t = 60.9$ (dashed line) orbital periods.

as in the previous three-dimensional simulations, but we are now using 128×255 grid points. The initial state is a stratified Keplerian accretion disc to which we have added a radial motion with amplitude 0.095, and a small random perturbation of the pressure. Initially the amplitude of the epicyclic motion, $\tilde{u}$, is constant, but the damping sets in suddenly after five orbital periods (Fig. 14). Over four orbital periods the amplitude of the epicyclic motion decreases by 30 per cent, after which the damping becomes weaker again. This is clearly not an exponential damping. At the same time as the epicyclic motion is damped, the vertical velocity starts to grow. The inertial waves themselves are not capable of transporting mass, but the parametric decay heats the central part of the disc, and the corresponding pressure increase pushes matter away from the mid-plane (Fig. 15).

The same parametric decay may be found in Run 4 (Fig. 13), which is done on the same grid as Run 3, but starting from a laminar state with only the epicyclic shear flow. In Run 3 the parametric decay occurs between orbits 58 and 60 (Fig. 16), but it is followed by an exponential damping caused by the turbulence itself (Fig. 7). The damping rate for Run 3 as estimated in Section 3.2 is based on a time interval after the end of the episode of parametric decay, and therefore represents the turbulent damping rate. Also, in Runs 3 and 4 we find an enhanced heating of the central regions of the disc and a resulting density reduction (Fig. 17).

4.2 Application to warped accretion discs

We now investigate the implications of our results for the large-scale dynamics of a warped accretion disc. In linear theory we may estimate the amplitude of the epicyclic motion as (cf. equation 18)

$$\frac{u_0}{c_s} \sim \frac{A}{\alpha_v}, \tag{30}$$

where A is the dimensionless amplitude of the warp. This estimate is valid for a thin and sufficiently viscous disc, that is for $H/r \lesssim \alpha_v \ll 1$ (Papaloizou & Pringle 1983). For observable warps in which A exceeds the aspect ratio of the disc, the epicyclic velocities are comparable to, or greater than, the sound speed, as is the case in our numerical simulations. Based on the high velocities, one might expect shocks to appear in the simulations, and shocks do appear in some global simulations that allow horizontal gradients in the epicyclic velocity (cf. Nelson & Papaloizou 1999). However, because of the local nature of our model we do not find any such gradients or shocks.

The large-scale dynamics of a warped disc has been formulated by Pringle (1992) in terms of two effective kinematic viscosity coefficients: ν_1 describes the radial transport of the component of the angular momentum vector parallel to the tilt vector, while ν_2 describes the transport of the perpendicular components. The relation between ν_1 and ν_2 and α is non-trivial but has been explained by Papaloizou & Pringle (1983) and Ogilvie (1999). Recall that α_h and α_v are effective viscosity parameters that represent the transport of momentum by turbulent motions (and magnetic fields) on scales small compared to H. Now $\nu_1 \propto \alpha_h$ as expected, because the parallel component of angular momentum is transported mainly by these small-scale motions and magnetic fields. However, $\nu_2 \propto \alpha_v^{-1}$ instead of the intuitive result $\nu_2 \propto \alpha_v$. (Here we assume $H/r \lesssim \alpha_v \ll 1$.) This is because the perpendicular components of angular momentum are transported mainly by the systematic epicyclic motions induced by the warp, and these are proportional to α_v^{-1} as explained in Section 2.3. In effect, ν_2 is an effective viscosity coefficient removed by an additional level from the turbulent scales. If we generalize the linear theory of Papaloizou & Pringle (1983) to allow for an anisotropic small-scale effective viscosity, we obtain $\nu_2/\nu_1 = 1/(2\alpha_h\alpha_v)$.

The condition for a warp to appear in the accretion disc is set by the balance between the torque that is exciting the warp and the viscous torque, described by ν_2, that is flattening the disc. The warp-exciting torque may for instance be a radiation torque from the central radiation source. Assuming that accretion is responsible for all the radiation, the radiation torque will depend on the viscosity ν_1. The criterion for the warp to appear will then depend on the ratio of viscosities $\eta = \nu_2/\nu_1$. Pringle (1996) showed that

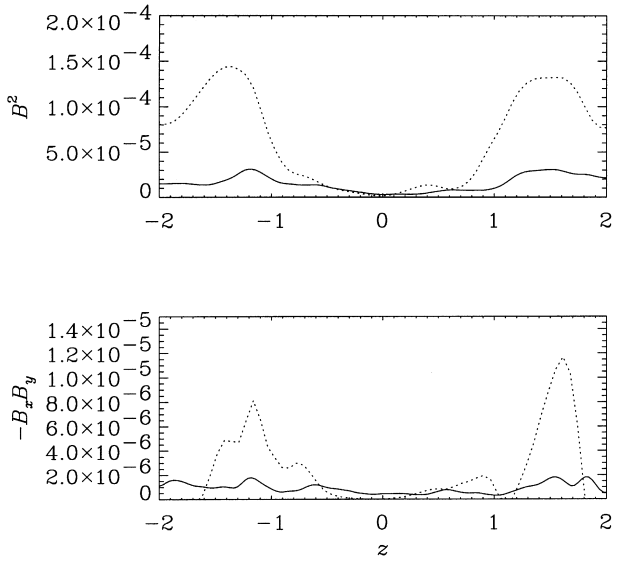

Figure 18. The upper plot shows $\overline{\langle B^2 \rangle}$, the average of the magnetic energy, as a function of z for Runs 3 at $66.3T_0$ (solid line) and 0 at $66.1T_0$ (dashed line). The lower plot shows $-\overline{\langle B_xB_y \rangle}$ plotted the same way.

an irradiation-driven warp will appear at radii

$$r \gtrsim \left(\frac{2\sqrt{2}\pi\eta}{\epsilon} \right)^2 R_{\rm Sch}, \tag{31}$$

where $R_{\rm Sch}$ is the Schwarzschild radius, and $\epsilon = L/\dot{M}c^2$ is the efficiency of the accretion process. We have shown that $\alpha_{\rm h} \approx \alpha_{\rm v} \ll 1$. However, we emphasize again that this does *not* imply that $\eta \approx 1$; on the contrary, we estimate that $\eta \approx 1/(2\alpha_{\rm h}\alpha_{\rm v}) \gg 1$. The high value for η will make it difficult for a warp to appear unless the radiation torque can be amplified by an additional physical mechanism. One way to produce a stronger torque is if the irradiation is driving an outflow from the disc (cf. Schandl & Meyer 1994).

A similar damping mechanism may affect waves excited by Lense–Thirring precession in the inner part of the accretion disc around a spinning black hole. Numerical calculations by Markovic & Lamb (1998) and Armitage & Natarajan (1999) show that these waves are damped rapidly unless $\nu_2 \ll \nu_1$, which we find is not the case. (However, we note that the resonant enhancement of ν_2 will be reduced near the innermost stable circular orbit, because the epicyclic frequency deviates substantially from the orbital frequency). Likewise a high value of ν_2 will lead to a rapid alignment of the angular momentum vectors of a black hole and its surrounding accretion disc (cf. Natarajan & Pringle 1998).

Some caution should be exercised when interpreting the results of this paper. Although the shearing box simulations in general have been successful in demonstrating the appearance of turbulence with the right properties for driving accretion, they are in general producing uncomfortably low values of $\alpha_{\rm h}$ to describe, e.g., outbursting dwarf nova discs (see Cannizzo, Wheeler & Polidan 1986). An underestimate of $\alpha_{\rm h}$ and $\alpha_{\rm v}$ would lead to an overestimate of η. In addition, the parametric instability leads to an enhanced damping of the epicyclic motion. If this effect had been sustained it would have resulted in a smaller value for η. In a warped accretion disc, the epicyclic motion is driven by the pressure gradients, which may maintain the velocities at a sufficient level for the parametric instability to operate continuously. To address this question we intend to study forced oscillations in a future paper.

4.3 The vertical structure of the accretion disc

Our previous simulations of turbulence in a Keplerian shearing box have shown that the turbulent xy stresses are approximately constant with height (Brandenburg et al. 1996) rather than proportional to the pressure as may have been expected from the α-prescription (Shakura & Sunyaev 1973). We modified the vertical boundary conditions for this paper and added an epicyclic motion. However, the $\langle B_xB_y \rangle$ stress is still approximately independent of z or even increasing with $|z|$ for $|z| < H$, while at larger $|z|$ we may see the effects of the boundary conditions (Fig. 18). The effect of the epicyclic motion is seemingly to limit the $\langle B_xB_y \rangle$ stress in the surface layers to its value in the interior of the disc. The fact that the stresses decrease more slowly with $|z|$ than does the density results in a strong heating of the surface layers.

5 CONCLUSIONS

In this paper we have studied how the turbulence in an accretion disc will damp an epicyclic motion, the amplitude of which depends on the vertical coordinate z in the accretion disc. Such a motion could be set up by a warp in the accretion disc (Papaloizou & Pringle 1983). We find that the typical damping time-scale of the epicyclic motion is about 25 orbital periods, which corresponds to $\alpha_{\rm v} = 0.006$. This value is comparable to the traditional estimate of $\alpha_{\rm h}$ that one gets from comparing the $\langle \rho u_x u_y - B_xB_y \rangle$ stress with the pressure. Both alphas are of the order of 0.01, which implies that the time-scale for damping a warp in the accretion disc is much shorter than the usual viscous time-scale. That the two alphas are within a factor of a few of each other is surprising, since the damping of the epicyclic motion may be attributed to the Reynolds stresses, while the accretion is mostly driven by the Maxwell stress.

However, not all of the damping can be described as a simple viscous damping. At high amplitudes the epicyclic motion may also decay parametrically to inertial waves. The damping is much more efficient in the presence of this mechanism.

ACKNOWLEDGMENTS

UT was supported by a European Union post-doctoral fellowship in Cambridge and is supported by the Natural Sciences Research Council (NFR) in Gothenburg. Computer resources from the National Supercomputer Centre at Linköping University are gratefully acknowledged. GIO is supported by the European Commission through the Training and Mobility of Researchers network 'Accretion on to Black Holes, Compact Stars and Protostars' (contract number ERBFMRX-CT98-0195). This work was supported in part by the Danish National Research Foundation hrough its establishment of the Theoretical Astrophysics Center (ÅN). RFS is supported by NASA grant NAG5-4031.

REFERENCES

Armitage P. J., Natarajan P., 1999, ApJ, 525, 909
Balbus S. A., Hawley J. F., 1991, ApJ, 376, 214
Balbus S. A., Hawley J. F., 1998, Rev. Mod. Phys., 70, 1

Brandenburg A., 1999, in Abramowicz M. A., Björnsson G., Pringle J. E., eds, Theory of black hole accretion discs. Cambridge Univ, Press, Cambridge, p. 61
Brandenburg A., Nordlund Å., Stein R. F., Torkelsson U., 1995, ApJ, 446, 741
Brandenburg A., Nordlund Å., Stein R. F., Torkelsson U., 1996, in Kato S. et al., eds, Basic physics of accretion disks. Gordon & Breach, New York, p. 285
Cannizzo J. K., Wheeler J. C., Polidan R. S., 1986, ApJ, 301, 634
Chandrasekhar S., 1960, Proc. Nat. Acad. Sci., 46, 253
Gammie C. F., Goodman J., Ogilvie G. I., 2000, MNRAS, in press (astro-ph/0001539)
Hawley J. F., Gammie C. F., Balbus S. A., 1995, ApJ, 440, 742
Hawley J. F., Gammie C. F., Balbus S. A., 1996, ApJ, 464, 690
Katz J. I., 1973, Sci, 246, 87
Markovic D., Lamb F. K., 1998, ApJ, 507, 316
Matsumoto R., Tajima T., 1995, ApJ, 445, 767
Miyoshi M., Moran J., Herrnstein J., Greenhill L., Nakai N., Diamond P., Inoue M., 1995, Nat, 373, 127
Natarajan P., Pringle J. E., 1998, ApJ, 506, L97
Nelson R. P., Papaloizou J. C. B., 1999, MNRAS, 309, 929
Nordlund Å., Stein R. F., 1990, Comput. Phys. Commun., 59, 119
Ogilvie G. I., 1999, MNRAS, 304, 557
Papaloizou J. C. B., Lin D. N. C., 1995, ApJ, 438, 841
Papaloizou J. C. B., Pringle J. E., 1983, MNRAS, 202, 1181
Pringle J. E., 1992, MNRAS, 258, 811
Pringle J. E., 1996, MNRAS, 281, 357
Roberts W. J., 1974, ApJ, 187, 575
Schandl S., Meyer F., 1994, A&A, 289, 149
Shakura N. I., Sunyaev R. A., 1973, A&A, 24, 337
Stone J. M., Hawley J. H., Gammie C. F., Balbus S. A., 1996, ApJ, 463, 656
Tananbaum H., Gursky H., Kellogg E. M., Levinson R., Schreier E., Giacconi R., 1972, ApJ, 174, L143
Terquem C. E. J. M. L. J., 1998, ApJ, 509, 819
Velikhov E. P., 1959, J. Exp. Theor. Phys., 9, 995 (Sov. Phys., 36, 1398 in Russian original)

This paper has been typeset from a TEX/LATEX file prepared by the author.